JACS
JOURNAL OF THE AMERICAN CHEMICAL SOCIETY
Article
pubs.acs.org/JACS

Development of a Robust Model System of FRET using Base Surrogates Tethering Fluorophores for Strict Control of Their Position and Orientation within DNA Duplex

Tomohiro Kato,[†] Hiromu Kashida,*[,†] Hideo Kishida,[†] Hiroyuki Yada,[‡] Hiroshi Okamoto,[‡] and Hiroyuki Asanuma*[,†]

[†]Graduate School of Engineering, Nagoya University, Furo-cho, Chikusa-ku, Nagoya 464-8603, Japan
[‡]Department of Advanced Materials Science, The University of Tokyo, 5-1-5 Kashiwanoha, Kashiwa, Chiba 277-8561, Japan

Supporting Information

ABSTRACT: Although distance dependence of Förster resonance energy transfer (FRET) is well-studied and FRET has been extensively applied as "molecular ruler", only limited examples of orientation-dependent FRET have been reported. To create a robust FRET system that precisely reflects the orientation between donor and acceptor, donor and acceptor fluorophores were introduced into a DNA via a D-threoninol scaffold. Strong stacking interactions among intercalated dyes and natural base-pairs suppress free movement of the dyes, clamping them in the duplex in a fixed orientation. Pyrene and perylene were used as donor and acceptor, respectively, and both the distance and orientation between these dyes were systematically controlled by varying the number of intervening AT pairs from 1 to 21 (corresponding to two turns of helix). FRET efficiency determined from static fluorescence measurement did not decrease linearly with the number (n) of inserted AT pairs but dropped significantly every 5 base pairs (i.e., n = 8, 13, and 18), corresponding to a half-turn of the B-type helix. This clearly demonstrates that FRET efficiency reflects the orientation between pyrene and perylene. We also measured time-resolved fluorescence spectroscopy with a streak camera and successfully observed the time-course of the energy transfer directly. As expected, the FRET efficiencies determined from the lifetime of pyrene emission were in good agreement with static measurements. Theoretical calculation of FRET efficiency assuming that the DNA duplex is a rigid cylinder with B-type geometry coincided with the experimental results. We believe that our method of using D-threoninol will contribute to further development of FRET-based measurement techniques.

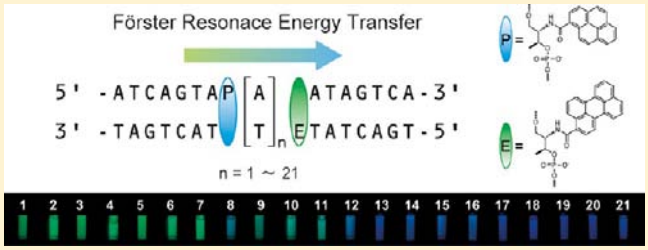

INTRODUCTION

Förster resonance energy transfer (FRET) is a physical phenomenon in which excited energy of a donor fluorophore is transferred to an acceptor nonradiatively.[1] FRET is widely utilized as a "molecular ruler" for studying the structure and interactions of macromolecules, such as proteins and nucleic acids,[2,3] since the efficiency of FRET depends on both distance and orientation between donor and acceptor. FRET techniques are used to monitor changes in distance of nano materials or biomolecules (e.g., DNA origami,[4] molecular probes,[5] molecular sensors,[6] ribozymes[7,8]). Advantages of FRET techniques include (1) high-sensitive fluorescent detection due to extended apparent Stokes' shift; (2) accurate measurement of distance over wide range (10−100 Å); and (3) the ability to monitor molecular dynamics using time-resolved fluorescence spectroscopy. However, in many cases, only distance dependence is taken into consideration, and orientation is assumed to be averaged owing to free rotation of chromophores.

FRET arises from a coupling of transition dipole moments of the dyes. The efficiency of FRET (Φ_T) and its related parameters is given by following equations:[9,10]

$$\Phi_T = \frac{1}{1 + (R/R_0)^6} \quad (1)$$

$$R_0 = 0.2108[J(\lambda)\kappa^2 n^{-4}\Phi_D]^{1/6} \quad (2)$$

$$\kappa^2 = (\cos\theta_T - 3\cos\theta_D\cos\theta_A)^2 \quad (3)$$

In eq 1, R is the separation distance between donor and acceptor, and R_0 is the distance, where Φ_T = 0.5, known as Förster radius. Efficiency decreases inversely with the sixth power of the distance, resulting in a significant drop of Φ_T around R_0. R_0 can be calculated from spectral overlap using a data set of donor emission and acceptor absorption (eq 2), where $J(\lambda)$ is spectral overlap at λ (nm). Φ_D is the quantum yield of the donor, and n is refractive index, typically assumed to be 1.4 for biomolecules in aqueous solution.[10] κ^2 is the orientation factor given by eq 3, where θ_T is the total angle of transition dipole moment between donor and acceptor, and θ_D and θ_A are the angles versus distant axis of donor and acceptor, respectively. In principle, FRET efficiency should depend on the mutual orientation (i.e., angle) between the donor and acceptor as well as their distance. However, under conditions in

Received: September 19, 2012
Published: December 14, 2012

dx.doi.org/10.1021/ja309279w | J. Am. Chem. Soc. 2013, 135, 741−750

which fluorophores freely move, the orientation factor is assumed to be an averaged value, $\kappa^2 = 2/3$.

DNA is an ideal scaffold for demonstrating orientation dependence of FRET because DNA forms a rigid double-helical structure.[11−19] Generally, the dyes are attached at termini or within grooves of DNA through long flexible linkers, and therefore FRET is assumed to be dependent on distance but not orientation as donor and acceptor should move freely.[20−26] Lewis et al. were first to report orientation-dependent FRET with a capped hairpin system where perylene was attached at a terminus of stilbene-linked hairpin DNA.[20] In this system, chromophores are stacked on base pairs, and FRET efficiency changed depending on the chromophore orientation. Iqbal et al. introduced fluorescent dyes at each end of DNA duplex; $\pi-\pi$ stacking of Cy3 and Cy5 at either end of duplex restricted free rotation of chromophores;[21] however, stacking onto the end of a DNA duplex tends to slip, and thus the orientation of dye was not sufficiently controlled. In addition, in these end-capped systems, it was difficult to interrogate short distances because of the instability of short duplexes. Börjesson et al. designed another excellent FRET system with fluorescent nucleic acid analogs mimicking deoxycytosine.[26] Since stacking interactions and hydrogen bonding allowed strict control of the position, they successfully observed the orientation-dependent FRET. However, this design is limited to fluorescent nucleic acid analogs.

Herein, we propose a novel FRET system in which fluorophores are incorporated as base surrogates using a D-threoninol scaffold.[27] Pyrene (P) and perylene (E), a well-characterized donor−acceptor pair,[13,28,29] were covalently inserted at desired positions (Figure 1a), as we described previously.[27,30,31] There are several advantages to this design. First, chromophores on D-threoninol facilitate intercalation between the nucleobases,[30] which inhibits not only free rotation of the dyes but also slip and slide, tilt and roll. Second, donor−acceptor pairs can be incorporated into any position of a DNA duplex. Hence, the distance and orientation between dyes could be readily controlled and estimated from well-known DNA structure parameters. Third, various dyes available as FRET pairs can be covalently tethered to the D-threoninol linker.

In this paper, we systematically investigated the orientation dependence of FRET from pyrene to perylene. The distance and orientation were systematically varied by inserting 1−21 AT pairs between dyes, and FRET efficiencies were determined both by static fluorescence measurement and time-resolved fluorescent spectroscopy. Comparison with theoretical values calculated based on a cylinder model of DNA is also discussed.

MATERIALS AND METHODS

Materials. All the conventional phosphoramidite monomers, CPG columns, reagents for DNA synthesis, and Poly-Pak II cartridges were purchased from Glen Research. Other reagents for the synthesis of phosphoramidite monomers were purchased from Tokyo Chemical Industry, Wako, and Aldrich. Native oligodeoxyribonucleotides (ODNs) were purchased from Integrated DNA Technologies.

Synthesis of Pyrene- and Perylene-Containing DNA. All dye-conjugated ODNs were synthesized on an automated DNA synthesizer (H-8-SE, Gene World) by using phosphoramidite monomers bearing P or E. Syntheses of P and E were reported previously.[33,34] After workup, synthesized ODNs were purified by reversed phase HPLC and characterized using a MALDI-TOF MS (Autoflex II, Bruker Daltonics). Purities of all the synthesized ODNs were >99% as estimated by HPLC analysis.

MALDI-TOFMS Data for the Synthesized ODNs. The MS data for ODNs (Figure 1b) were as follows: m/z: **1a**: calcd for [**1a** + H^+]: 4977: found: 4978; **1b**: calcd for [**1b** + H^+]: 5000: found: 5001; **2a**: calcd for [**2a** + H^+]: 5290: found: 5292; **2b**: calcd for [**2b** + H^+]: 5304: found: 5307; **3a**: calcd for [**3b** + H^+]: 5603: found: 5606; **3b**: calcd for [**3b** + H^+]: 5608: found: 5609; **4a**: calcd for [**4a** + H^+]: 5916: found: 5919; **4b**: calcd for [**4b** + H^+]: 5912: found: 5918; **5a**: calcd for [**5a** + H^+]: 6229: found: 6231; **5b**: calcd for [**5b** + H^+]: 6216: found: 6217; **6a**: calcd for [**6a** + H^+]: 6542: found: 6547; **6b**: calcd for

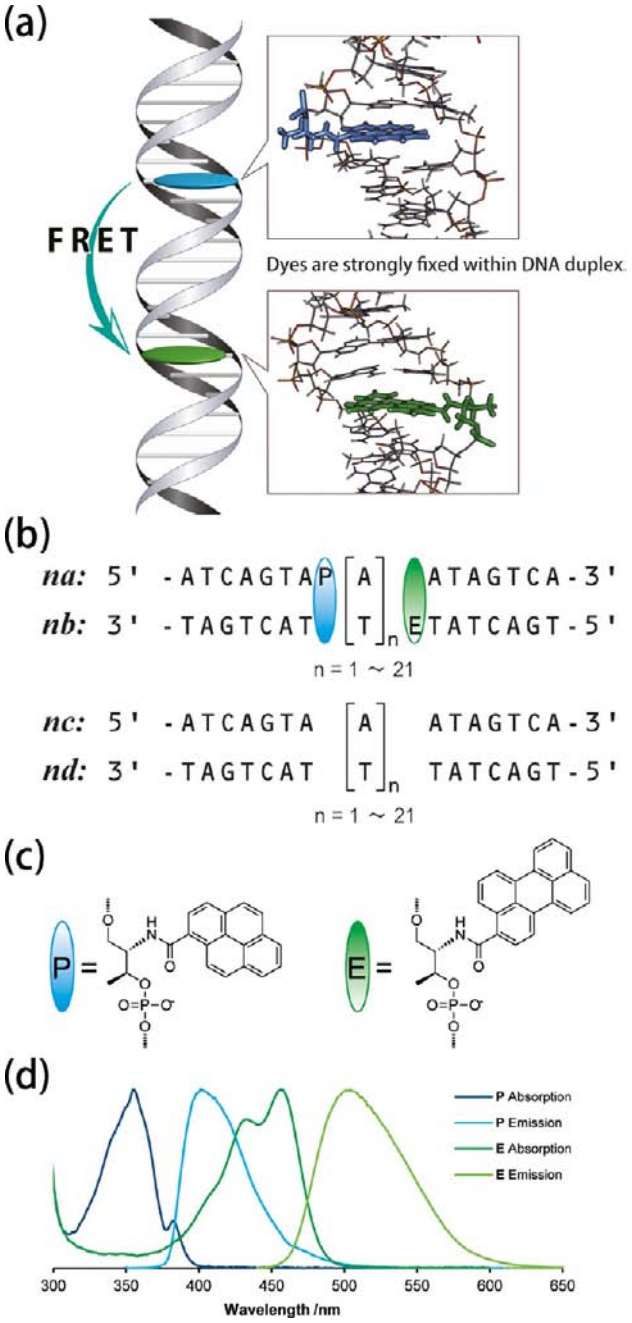

Figure 1. Schematic of FRET system used in this study. (a) Graphical representation of our FRET system. (b) Sequence of FRET ODN pair. AT pairs were inserted between P (pyrene as donor) and E (perylene as acceptor). P and E moieties were introduced into strands *na* and *nb*, respectively, where *n* indicates the number of inserted A or T residues; *nc* and *nd* were ODNs without fluorophores with sequences identical to *na* and *nb*, respectively. P and E moieties are inserted into the DNA duplex as single-residue bulges when *na* and *nb* are hybridized. (c) Structure of P and E. Fluorophores were directly conjugated via D-threoninol to the DNA strand. (d) Absorption and emission spectra of P and E.

dx.doi.org/10.1021/ja309279w | J. Am. Chem. Soc. 2013, 135, 741−750

[**6b** + H^+]: 6520: found: 6524; **7a**: calcd for [**7a** + H^+]: 6855: found: 6858; **7b**: calcd for [**7b** + H^+]: 6824: found: 6828; **8a**: calcd for [**8b** + H^+]: 7168: found: 7170; **8b**: calcd for [**8b** + H^+]: 7128: found: 7131; **9a**: calcd for [**9a** + H^+]: 7481: found: 7480; **9b**: calcd for [**9b** + H^+]: 7432: found: 7433; **10a**: calcd for [**10a** + H^+]: 7795: found: 7798; **10b**: calcd for [**10b** + H^+]: 7736: found: 7741; **11a**: calcd for [**11a** + H^+]: 8108: found: 8111; **11b**: calcd for [**11b** + H^+]: 8040: found: 8047; **12a**: calcd for [**12a** + H^+]: 8421: found: 8427; **12b**: calcd for [**12b** + H^+]: 8345: found: 8349; **13a**: calcd for [**13a** + H^+]: 8734: found: 8740; **13b**: calcd for [**13b** + H^+]: 8649: found: 8651; **14a**: calcd for [**14a** + H^+]: 9047: found: 9049; **14b**: calcd for [**14b** + H^+]: 8953: found: 8955; **15a**: calcd for [**15a** + H^+]: 9360: found: 9366; **15b**: calcd for [**15b** + H^+]: 9257: found: 9263; **16a**: calcd for [**16a** + H^+]: 9673: found: 9674; **16b**: calcd for [**16b** + H^+]: 9561: found: 9863; **17a**: calcd for [**17a** + H^+]: 9986: found: 9988; **17b**: calcd for [**17b** + H^+]: 9865: found: 9869; **18a**: calcd for [**18a** + H^+]: 10299: found: 10305; **18b**: calcd for [**18b** + H^+]: 10169: found: 10178; **19a**: calcd for [**19a** + H^+]: 10612: found: 10614; **19b**: calcd for [**19b** + H^+]: 10473: found: 10475; **20a**: calcd for [**20a** + H^+]: 10925: found: 10930; **20b**: calcd for [**20b** + H^+]: 10777: found: 10779; **21a**: calcd for [**21a** + H^+]: 11238: found: 11243; **21b**: calcd for [**21b** + H^+]: 11081: found: 11087.

Spectroscopic Measurements. Fluorescence spectra were measured on a JASCO model FP-6500 equipped with a micro cell holder. The excitation wavelength was 345 nm. For FRET analyses, experiments were conducted at 20 °C. Before measurement, sample solutions containing DNA duplex were heated at 80 °C, then slowly cooled down to 20 °C by programmable temperature controller. The temperature ramp was 4 °C min^{-1}.The sample solutions were as follows: 100 mM NaCl, 10 mM phosphate buffer, pH 7.0, 1.0 μM each DNA strand. Measurement error of fluorescence intensity was within ±1.5%. UV−vis spectra were measured in a 10 mm quartz cell on a JASCO model V-530 or V-560 equipped with programmed temperature controller. The sample solutions were as follows: 100 mM NaCl, 10 mM phosphate buffer, pH 7.0, 5.0 μM each DNA strand. CD spectra were measured in a 10 mm quartz cell on a JASCO model J-820 equipped with programmable temperature controllers. The sample solutions were as follows: 100 mM NaCl, 10 mM phosphate buffer, pH 7.0, 4.0 μM each DNA strand.

Measurement of the Melting Temperature (T_m). The melting curve of duplex DNA was obtained with a Shimadzu UV-1800 by measurement of the change in absorbance at 260 nm versus temperature. The temperature ramp was 0.5 °C min^{-1}. The sample solutions were as follows: 100 mM NaCl, 10 mM phosphate buffer, pH 7.0, 5.0 μM each DNA strand.

Analysis of Time-Resolved Fluorescence Using a Streak Camera. A pulse at 780 nm was generated by a Ti:sapphire amplified laser system Integra-C (Quantronix, 130 fs, 1 kHz). The pulse was changed to a 1380 nm pulse by an optical parametric amplifier (Topas, Light Conversion). The excitation beam had a repetition rate of 1 kHz and a pulse width of 130 fs and was converted to 345 nm through SHG crystals twice and band-pass filters. Fluorescence emission was captured by a streak camera (Hamamatsu C4334) operating in photon counting mode. Measurements were performed at room temperature. The sample solutions contained 100 mM NaCl, 10 mM phosphate buffer, pH 7.0, 50 μM each ODN *na* and *nb*. The sample solution was placed into a quartz cell with a screw cap (1 mm optical path length, 10 mm width) in order to adjust the absorbance at 345 nm equals to ∼0.1.

Curve Fitting Calculation. The fluorescence decay of P was fitted using the U8167-01 program (Hamamatsu). For n = 1−12, shorter time-scale data of 10 ns was used, and a longer time scale of 50 ns was applied for n = 13−21. Decay curves of P and E were obtained from integration of the region from 384.6 to 439.0 nm and from 469.8 to 603.2 nm, respectively. Signal counts were normalized by setting maxima to 1000 and plotted on semilogarithmic scale. The donor decay was assumed with the typical single- or biexponential function of $\alpha_1 \exp(-t/\tau_1) + \alpha_2 \exp(-t/\tau_2)$. Fluorescence decay of E, the population of excited acceptor was estimated by the step reaction as follows:

$$[P^*] \xrightarrow{k_E} [E^*] \xrightarrow{k_D} [E] \quad (4)$$

Here, k_E shows the rate constant of energy transfer from P to E, and k_D is the rate constant of radiative decay of E. The population of excited acceptor E* was estimated from fluorescence decay of E according to the step reaction equation of $[k_E/(k_D - k_E)]\ [\exp(-k_E t) - \exp(-k_D t)]$. Curve fitting of E was performed on Kaleida Graph ver. 4.0 (Synergy Software).

Calculation of Transition Dipole Moment. The transition dipole moments of P and E were calculated using an *ab initio* quantum mechanical method in the Gaussian 09W suite of programs. The optimized excited-state geometries and transition dipole moments of P and E were calculated at the TDDFT B3LYP 6-31G level.

Molecular Modeling. The Insight II/Discover 98.0 program package was used for conformational energy minimization. The FRET pair n = 10 was built from canonical B-form DNA by a graphical program. The AMBER95 force field was used for the calculation. All the structures were energy minimized to an RMS derivative of <0.001 kcal $Å^{-1}$. Computations were carried out on a Silicon Graphics O2+ workstation with the IRIX64 OS release 6.5.

Calculation of FRET Efficiency. In this study, FRET efficiency was calculated by three methods. FRET efficiency Φ_{T1} (decrease in donor emission), Φ_{T2} (increase in acceptor emission), and Φ_{T3} (donor decay lifetime) were calculated with following equations:

$$\Phi_{T1} = 1 - I_{DA,400}/I_D \quad (5)$$

where $I_{DA,400}$ is emission intensity of FRET pair *na*/*nb* at 400 nm, and I_D is that of donor only duplex *na*/*nd* at 400 nm.

$$\Phi_{T2} = [A_A/A_D][I_{DA,530}/I_A - 1] \quad (6)$$

where A_A and A_D are absorbance of acceptor and donor at 345 nm, respectively, $I_{DA,530}$ is emission intensity of FRET pair *na*/*nb* at 530 nm, and I_A is that of acceptor only duplex *nc*/*nb* at 530 nm.

$$\Phi_{T3} = 1 - \tau_{DA}/\tau_D \quad (7)$$

where τ_{DA} is the lifetime of P in *na*/*nb*, and τ_D is the lifetime of P in the duplex without acceptor 11*a*/11*d*. The lifetime of P in duplex 11*a*/11*d* was 9.07 ns for n = 1−12 and 9.61 ns for n = 13−21.

RESULTS AND DISCUSSION

Strategy and Design of the FRET System. The basic FRET system designed in this study is shown in Figure 1a,b. We synthesized 21 ODN sets that contained from 1 to 21 AT pairs between donor and acceptor. The number of base pairs between donor and acceptor affects both distance and orientation between FRET pairs. Sequences at either end of the ODNs facilitate exact base pairing and rigid duplex formation. These conserved sequences were carefully designed to avoid undesired intra- or intermolecular structures.

Donor and acceptor were introduced into ODNs *na* and *nb*, respectively. ODNs without fluorophores, *nc* and *nd*, were also synthesized. Control duplexes tethering only a donor or acceptor were prepared by hybridizing pairs *na*/*nd* or *nc*/*nb*. We chose 1-pyrenecarboxylic acid (P) and 3-perylenecarboxylic acid (E) as donor and acceptor, respectively (Figure 1c). These fluorophores are photochemically stable, and their planar structures are suitable for the intercalation into a DNA duplex. These chromophores were introduced into DNA strands via D-threoninol scaffolds as previously described.[27,30] P and E were directly conjugated to D-threoninol in order to suppress free movement of dyes once incorporated into duplex. FRET efficiency depends on the quantum yield of the donor, which is responsible for R_0; P has a high quantum yield of 0.5. (This value is consistent with a similar pyrene derivative reported in ref 35 and determined by using 9,10-biphenylanthracene in EtOH (0.95) as a reference.) The spectral overlap of donor (P) emission and acceptor (E) absorption ($J(\lambda)$) was calculated as 4.50×10^{14} (M^{-1} cm^{-1} nm^4) (Figure 1d). Based on these parameters, we obtained an R_0 of 38.8 Å (when $\kappa^2 = 2/3$) for our FRET system. This value approximately corresponds to n = 11.

dx.doi.org/10.1021/ja309279w | J. Am. Chem. Soc. 2013, 135, 741−750

In this paper, we used pyrene and perylene as a typical example of donor and acceptor, respectively, by intervening only AT pairs between them to avoid fluorescence quenching of P by GC pair (see Figure S6). FRET also occurred even though GC pair was located in proximity of donor, although Förster radius should decrease due to low quantum yield of the donor. Note that other dyes pairs are also applicable with D-threoninol as a scaffold. By choosing appropriate donor–acceptor pairs, both Förster radius and excitation (emission) wavelength would be controllable in our system.

Spectroscopic Behavior of ODN-Dye Conjugates. We first measured UV–vis and CD spectra in order to investigate the structure of the duplexes modified with dyes. Figure 2

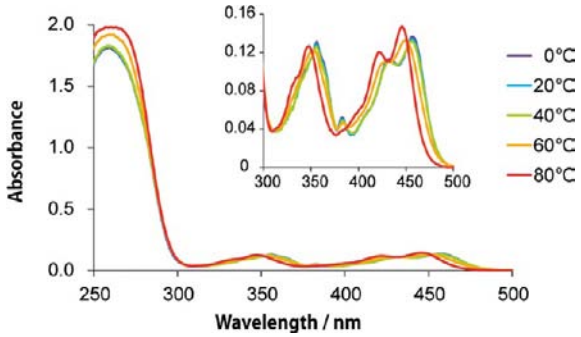

Figure 2. Temperature dependence of UV–vis spectra of 10*a*/10*b*. Solution conditions were as follows: 100 mM NaCl, 10 mM phosphate buffer, pH 7.0, 5.0 μM each ODN.

shows the temperature dependence of UV–vis spectra of n = 10 FRET system (10*a*/10*b*). At 80 °C, an absorption maximum (λ_{max}) of pyrene was observed at 348 nm, while that of perylene appeared at 445 nm. When the temperature was decreased to 0 °C, ODNs formed a duplex, and the λ_{max}s of pyrene and perylene shifted to 356 and 457 nm, respectively. These red shifts at lower temperature indicated that the dyes were intercalated within DNA duplex.[36] Melting temperature (T_m) analyses also supported the intercalation of P and E moieties (Table 1). The duplex containing P and E moieties (*na*/*nb*) had a higher T_m than the control duplex without dyes (*nc*/*nd*), indicating duplexes were stabilized through stacking interactions between dyes and natural base pairs. We also measured CD spectra of 18*a*/18*b* and the control native DNA duplex, 18*c*/18*d* (Figure S1). Very weak signals were observed from 18*a*/18*b* at around 350 nm (P) and 450 nm (E). These induced CD signals also support intercalation of dyes. Note that induced CD of intercalated dye is usually weak.[37] In addition, complicated couplets were observed at around 260 nm due to the AT tract. This unique signal near 260 nm was also observed[38] in the 18*c*/18*d* duplex, indicating that the structure of surrounding base pairs is not disturbed by the introduction of dyes. These observations are consistent with our previous NMR analyses that revealed that a planar *trans*-azobenzene on D-threoninol is intercalated between the base pairs.[30,32] Thus, structural perturbation by the modification with base surrogates is minimal, and we can assume that the FRET system adopts a typical B-type DNA structure.

Static Measurement of Fluorescence Spectra. Static fluorescence spectra of FRET duplexes were measured. Figure 3 shows fluorescence spectra of duplexes with n = 5, 10, 15, and 20. Blue emission around 400 nm and green emission around 500 nm result from donor (P) and acceptor (E), respectively. In the case of n = 5, the emission intensity of donor was significantly less than that of the acceptor emission. In contrast, for n = 20, acceptor emission was very weak, and donor emission was highly intense. Duplexes with n = 10 and n = 15 had intensities between those of the n = 5 and 20 duplexes. These spectral changes could be clearly observed with naked eyes (Figure 4a). Figure 4 shows fluorescence intensities of pyrene and perylene in *na*/*nb* duplexes. The decrease of donor emission and the increase of acceptor emission were highly correlated. Interestingly, the distance dependence of these emissions was not monotonous (Figure 4b,c). The periodical change in orientation factor as a function of the number of inserted AT pairs induced measurable changes of FRET efficiency. When n = 8, 13, and 18, a prominent decline of FRET efficiency was observed. This was visually observed as a color change in Figure 4a. For n = 8, the sample solution emitted bluish-green fluorescence, which was obviously different from green color of duplexes with n = 7 and 9. This cycle of about 5 bp reflected approximately half turns (180°) of the B-type DNA helix indicating that orientation of donor and acceptor was based upon DNA structure. This result is consistent with the previous reports by others.[23,26]

Time-Resolved Fluorescence Measurement. Periodical changes of FRET efficiency were also observed by time-resolved fluorescence measurements using a streak camera. Representative examples are shown in Figure 5. Both P and E had lifetimes of approximately 10 ns. Changes in FRET efficiency were visually apparent in the streak images. For example, for the duplex with n = 5 (Figure 5a), the signal of P around 400–450 nm disappeared within several ns since the FRET efficiency was very high. On the other hand, for duplexes with n = 15 and 20, the decay of P was longer due to lower FRET efficiency (Figure 5c,d). In addition, the time course of energy transfer was observed. In Figure 5b, the signal of E around 500–600 nm was delayed for several ns compared with the decay of P.

The lifetime of P was extracted from the streak figures (Figure 6a). Fluorescence lifetime of P was obviously changed with FRET efficiency. When the dyes were located in close proximity, fluorescence lifetimes were short due to efficient FRET (nonradiative process). As the dyes drew apart, lifetimes became longer and took almost the same value as that of the donor only lifetime. We also extracted lifetime of E to obtain more information of energy transfer (Figure 6b). For n = 5, energy transfer occurred within several ns, while slow ascent of fluorescence could be observed due to the slow energy transfer for n = 10. Then we obtained lifetime values from extracted fluorescence decay. All fitted parameters are summarized in Table 1. Decay curves of P exhibit two exponential curves when duplexes with n < 8 were analyzed, whereas those curves obtained from duplexes with $n \geq 8$ showed only single exponential curves. The shorter lifetime was caused by FRET, and the longer one was from the donor without energy transfer, as it is almost the same as a lifetime of the donor in the absence of the acceptor (9–10 ns). In addition, the rate constant calculated only from shorter lifetime (k_p) was consistent with that calculated from the acceptor emission (k_E; *vide infra*). Thus, we utilized only shorter lifetimes for the calculation of k_p and FRET efficiencies (Φ_{T3}). These biexponential decays might be caused by unhybridized strand or by experimental errors in measurement of the short lifetime. These fitting results were consistent even if the longer lifetime was fixed known value of donor decay (see Table S2). Similar biexponential decay was observed previously.[26,39] For the duplex n = 1, the

dx.doi.org/10.1021/ja309279w | J. Am. Chem. Soc. 2013, 135, 741–750

Table 1. Summary of the Results from T_m Measurement, FRET Efficiency Calculated from Static Measurement Data and Time-Resolved Measurement Data, and Fluorescence Lifetime Curve Fitting

n	T_m (ΔT_m), °C[a]	τ_1, ns[b]	α_1[b]	τ_2, ns[b]	α_2[b]	χ^2[b]	Φ_{T1}[c]	Φ_{T2}[d]	Φ_{T3}[e]	k_P, ns^{-1}[f]	k_E, ns^{-1}[g]
1	54.6 (+8.9)	n.d.	n.d.	n.d.	n.d.	n.d.	0.88	0.89	n.d.	n.d.	18.09
2	58.2 (+9.5)	0.08	0.97	8.80	0.03	1.33	0.95	1.03	0.99	12.82	8.02
3	57.3 (+8.5)	0.37	0.96	7.65	0.04	1.29	0.91	1.04	0.96	2.70	2.51
4	58.0 (+6.4)	0.27	0.98	8.60	0.02	1.37	0.90	0.80	0.97	3.75	3.53
5	57.9 (+6.6)	0.19	0.86	8.46	0.14	1.06	0.92	0.92	0.98	5.18	4.01
6	59.3 (+6.0)	0.36	0.95	6.43	0.05	1.11	0.87	0.85	0.96	2.77	2.67
7	60.9 (+7.0)	1.27	0.92	7.10	0.08	1.26	0.83	0.85	0.86	0.79	0.97
8	59.5 (+5.0)	5.73	1.00			1.43	0.43	0.43	0.37	0.17	0.30
9	60.9 (+5.3)	4.17	1.00			1.27	0.58	0.64	0.54	0.24	0.62
10	60.0 (+4.1)	3.51	1.00			1.29	0.63	0.65	0.61	0.28	0.38
11	61.9 (+5.6)	4.45	1.00			2.38	0.51	0.56	0.51	0.22	0.28
12	57.0 (+0.0)	6.46	1.00			2.32	0.31	0.30	0.29	0.15	0.28
13	62.7 (+5.5)	8.92	1.00			1.21	0.08	0.12	0.07	0.11	–
14	63.2 (+5.5)	8.20	1.00			1.35	0.18	0.15	0.15	0.12	–
15	60.6 (+2.6)	7.64	1.00			1.64	0.21	0.22	0.20	0.13	–
16	63.2 (+4.8)	8.28	1.00			0.99	0.15	0.18	0.14	0.12	–
17	63.0 (+4.3)	9.18	1.00			1.60	0.13	0.09	0.04	0.11	–
18	61.1 (+1.7)	9.27	1.00			1.69	0.05	0.08	0.04	0.11	–
19	63.5 (+4.0)	9.52	1.00			1.50	0.03	0.04	0.01	0.10	–
20	63.7 (+3.9)	9.27	1.00			1.64	0.03	0.08	0.04	0.11	–
21	62.7 (+2.5)	8.75	1.00			1.80	0.08	0.11	0.09	0.11	–

[a]Measurement conditions: 100 mM NaCl, 10 mM phosphate buffer, pH 7.0, 5.0 μM each ODN; 0.5 °C/min. ΔT_m was the difference between T_ms of *na*/*nb* and control duplexes without dyes (*nc*/*nd*). [b]Normalized counts were fitted with a biexponential curve of $\alpha_1 \exp(-t/\tau_1) + \alpha_2 \exp(-t/\tau_2)$. Where α is amplitude of lifetime component and τ is lifetime. χ^2 is chi-squared value obtained by the fitting program. [c]Donor decrease-based FRET efficiency given by $\Phi_{T1} = 1 - I_{DA,400}/I_D$ where $I_{DA,400}$ is emission intensity of FRET pair *na*/*nb* at 400 nm, and I_D is that of donor only *na*/*nb* at 400 nm. [d]Acceptor increase-based FRET efficiency given by $\Phi_{T2} = [A_A/A_D]\,[I_{DA,530}/I_A - 1]$ where A_A and A_D are absorbance of acceptor and donor at 345 nm, respectively, $I_{DA,530}$ is emission intensity of FRET pair *na*/*nb* at 530 nm, and I_A is that of acceptor only *nc*/*nb* at 530 nm. [e]Donor lifetime-based FRET efficiency given by $\Phi_{T3} = 1 - \tau_{DA}/\tau_D$ where τ_{DA} is lifetime of P in *na*/*nb* and τ_D is that of the duplex containing only donor 11*a*/11*d*. Fluorescence lifetime of the duplex containing only donor 11*a*/11*d* was 9.07 ns for n = 1–12 and 9.61 ns for n = 13–21. [f]Rate constant of donor decay given by $k_P = 1/\tau_1$. [g]Rate constant of acceptor rise (k_E) was calculated from acceptor decay fitting. For more information, see Materials and Methods section. For n > 12, emission of E could not be fitted correctly because of high background.

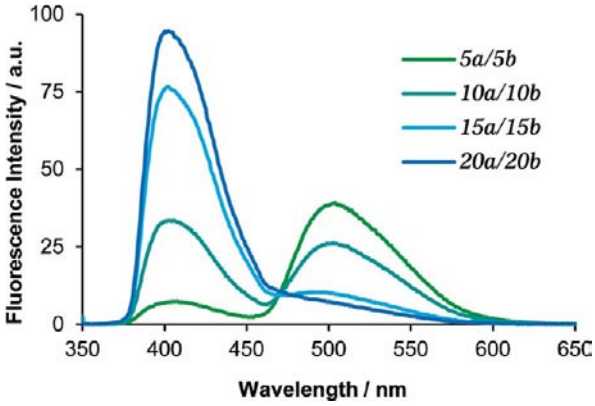

Figure 3. Fluorescence emission spectra of FRET pairs (n = 5, 10, 15, and 20) at 20 °C. The excitation wavelength was 345 nm. All the fluorescence spectra of FRET pairs and fluorescence spectra (n = 11) without donor or acceptor are depicted in Figures S2 and S3, respectively. Solution conditions were as follows: 100 mM NaCl, 10 mM phosphate buffer, pH 7.0, 1.0 μM each ODN. Before measurements, samples were heated at 80 °C for 5 min followed by cooling gradually at the rate of 4 °C/min to 20 °C.

lifetime of P was too short to observe, indicating that FRET efficiency was higher than 99%. As expected, k_P did not vary linearly with the distance. For duplexes with n = 8 and 13, the lifetimes were longer than those of adjacent duplexes (n = 8 vs n = 9 or 10, n = 13 vs n = 12 or 14), resulting in the decline of FRET efficiency. These results are totally consistent with static fluorescence measurement.

We also calculated the rate constant of FRET from acceptor emission (k_E). The increase in acceptor emission was fitted by assuming a step reaction and rate constants were obtained (Figure S4 and Table 1). Decay curves of the acceptor could not be fitted for longer duplexes (n > 12), probably due to weak acceptor emissions. Those rate constants that could be calculated were almost the same as the rate constants calculated from the donor emission (k_P).

Comparison of Experimental Data with Cylinder Model. FRET efficiency in DNA has been estimated based on a rigid cylinder model of the DNA helix (Figure 7).[11,40] Here, we supposed some values to simplify the theoretical calculation of FRET efficiency. The orientation and distance involving FRET efficiency was defined, as shown in Figure 7a. In our FRET system, the dyes were assumed to be in an almost parallel plane as dyes are intercalated within the DNA duplex. Based on this assumption, θ_D and θ_A in Figure 7a are 90° and the orientation factor κ^2 in eq 3, can be simplified:

$$\kappa^2 = \cos^2 \theta_T \quad (8)$$

Here, θ_T is the angle between dyes in rotational direction of helix. As described above, the distance and orientation of dyes periodically varied with the number of inserted AT pairs. As shown in Figure 7b, the distance between the dyes (R) increases by 3.2 Å/bp, which is slightly shorter than typical B-type DNA duplex owing to the influence of the AT tract.[17,41]

dx.doi.org/10.1021/ja309279w | J. Am. Chem. Soc. 2013, 135, 741–750

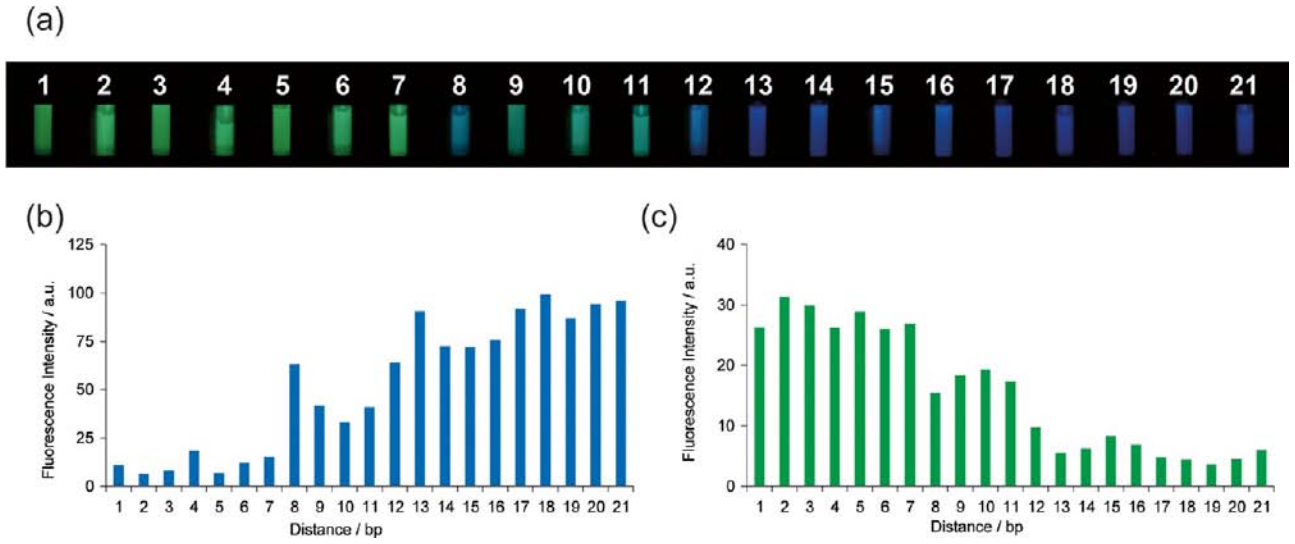

Figure 4. Distance dependence of fluorescence intensity of *na*/*nb* duplexes. (a) Photograph of samples excited at 340 nm. (b) Fluorescence intensity of P (400 nm) at 20 °C. The excitation wavelength was 345 nm. (c) Fluorescence intensity of E (530 nm). Measurement conditions are the same as those of Figure 3.

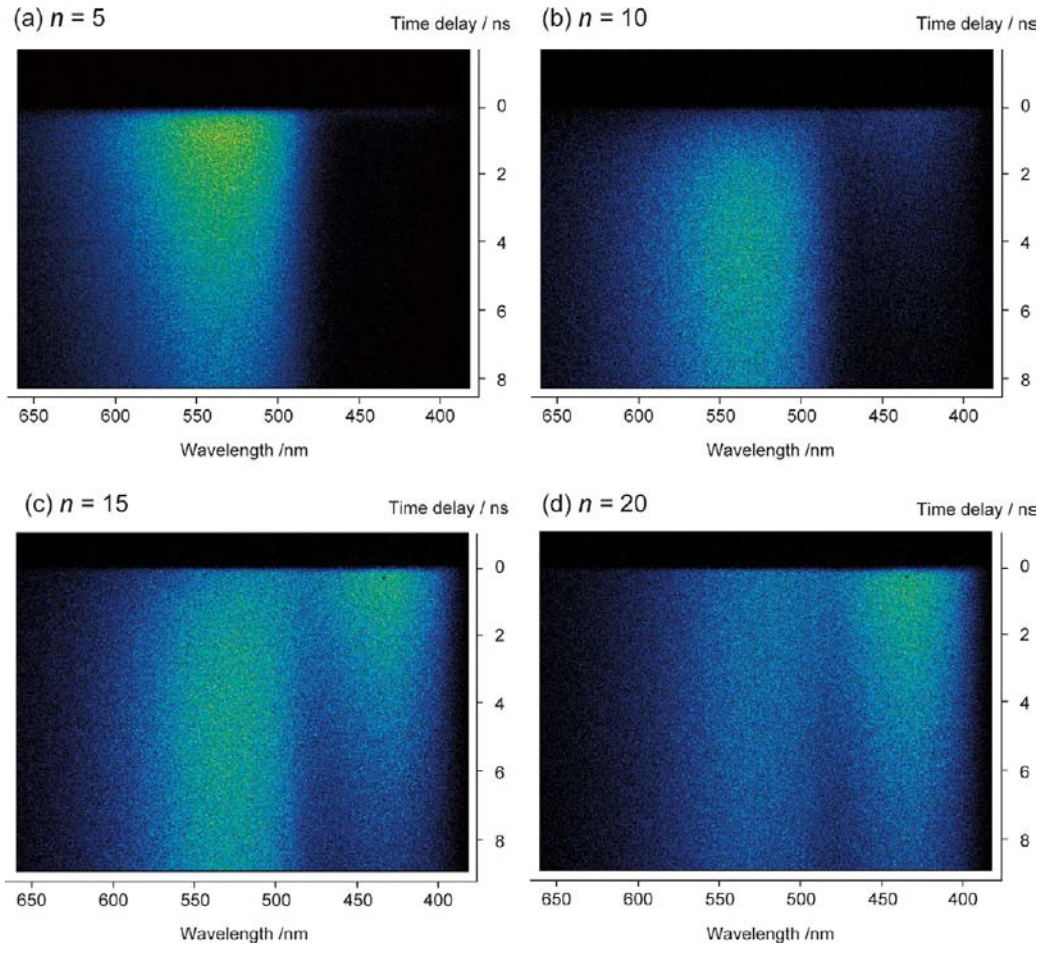

Figure 5. Streak images of *na*/*nb* (*n* = 5, 10, 15, and 20). Excitation wavelength was 345 nm. Solution conditions were as follows: 100 mM NaCl, 10 mM phosphate buffer, pH 7.0, 50 μM each ODN; room temperature.

The angle θ_T varies by −36°/bp (10 bp/turn). Dye angles owing to conjugation with D-threoninol should also be corrected. We determined the transition dipole moments of the two dyes by Gaussian 09W TD-DFT B3LYP 6-31G (Figure 7c) and found that the transition dipole moments of pyrene (P) and perylene (E) were parallel to the long axes of each dye.[42,43] Next, the angles between transition dipole moment and proximal AT pair were obtained from an energy minimized structure calculated by

dx.doi.org/10.1021/ja309279w | J. Am. Chem. Soc. 2013, 135, 741−750

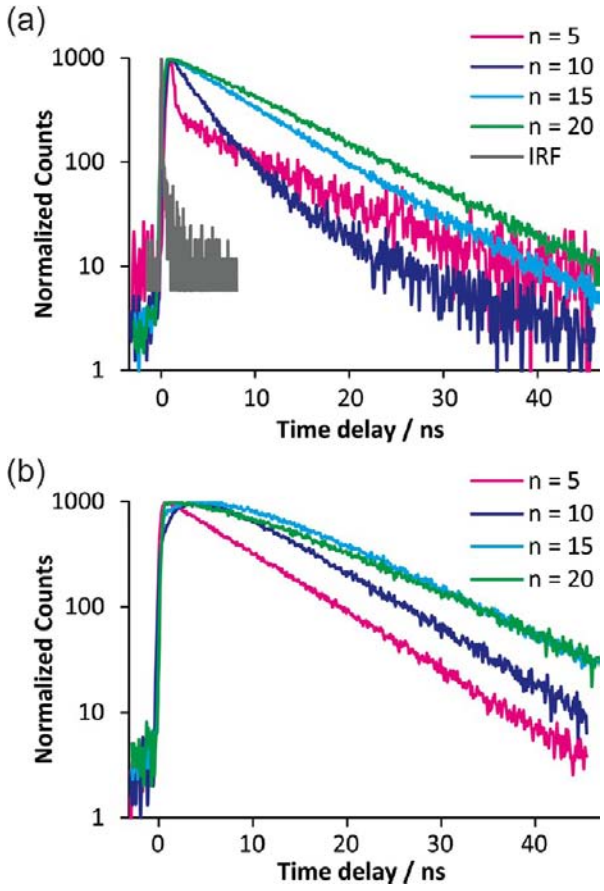

Figure 6. Fluorescence decay curves extracted from streak images. Signal counts were normalized by setting maxima to 1000 and plotted on semilogarithmic scale. (a) Decay curves of P obtained from integration of the region from 384.6 to 439.0 nm. Instrument response factor (IRF) is shown by the gray line. (b) Decay curves of E obtained from integration of the region from 469.8 to 603.2 nm.

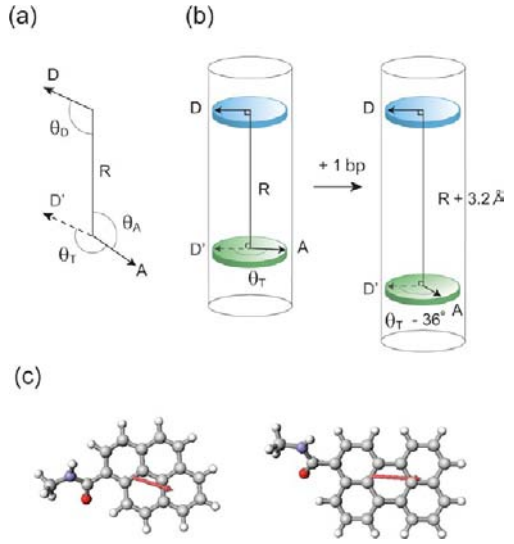

Figure 7. Illustrations of the cylinder model. (a) Assignment of angles for calculation of orientation factor. (b) Dyes are assumed to be completely parallel, and the helical axis was assumed to penetrate the center of each dye. Insertion of an AT pair affords +3.2 Å in distance and −36° in angle. (c) Calculated transition dipole moments of P and E by Gaussian 09W. Red arrows indicate the transition dipole moments.

computer simulation using the Insight II/Discover 98.0 program package. The angle from P to the proximal AT was nearly parallel (~0°), whereas that of E was about −25° (Figure 8b,c). Accordingly, orientation of dyes is given by the following equation:

$$\theta_T = -36° \times (n - 1) - 25° \quad (9)$$

And the distance R in Å is

$$R = 3.2 \times (n + 1) \quad (10)$$

Figure 8a shows the computational calculation of energy-minimized structure for the duplex with n = 10; dyes are located over a distance of 10 + 1 bp, namely, almost one turn of helix. The dye axes are parallel and intercalated between base pairs. When n = 10, θ_T was calculated to be −349°, which was consisted with simulated structure (Figure 8d).

The combination of eqs 1, 2, 8−10 allows calculation of FRET efficiency, Φ_T, of *na*/*nb* duplexes. For comparison of measured FRET efficiency with the cylinder model, FRET efficiency Φ_{T1} (decrease in donor emission), Φ_{T2} (increase in acceptor emission), Φ_{T3} (donor decay lifetime) were experimentally determined (Table 1). Observed FRET efficiencies obtained from the different methods showed similar dependency on the number of incorporated AT pairs (n), demonstrating the validity of this model. The exception was Φ_{T2} determined from the increase in acceptor emission, which had relatively large

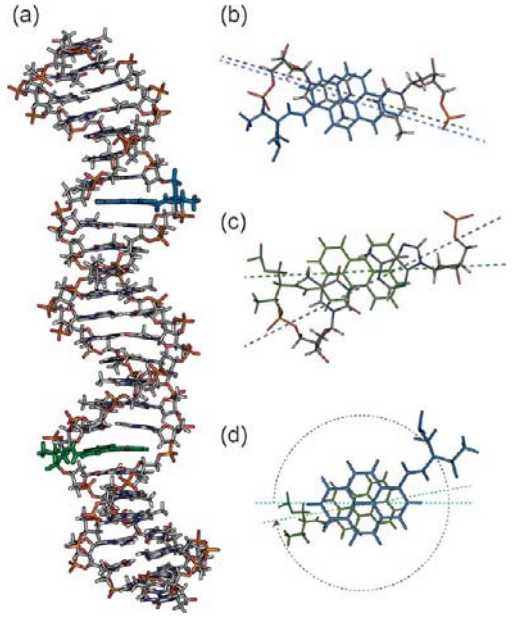

Figure 8. Computer simulation of energy minimized structure of FRET duplex with n = 10 by Insight II/Discover 98.0 program package. (a) Structure of duplex with FRET pair. P is indicated in blue, and E is indicated in green. (b) Angle between P and neighboring AT pair (0°). (c) Angle between E and neighboring AT pair (25°). (d) Total angle (θ_T) between P and E. The θ_T of −349° calculated based on the cylinder model was in good agreement with the computer simulation. Right-handed dashed arrow indicates −349°.

values compared with others, probably due to experimental difficulty in determining Φ_{T2} from small absorbances.

The comparison of experimental values with the calculated FRET efficiencies is shown in Figure 9. The experimental values are in excellent agreement with the calculated values, confirming the validity of the cylinder model. Determination

dx.doi.org/10.1021/ja309279w | J. Am. Chem. Soc. 2013, 135, 741−750

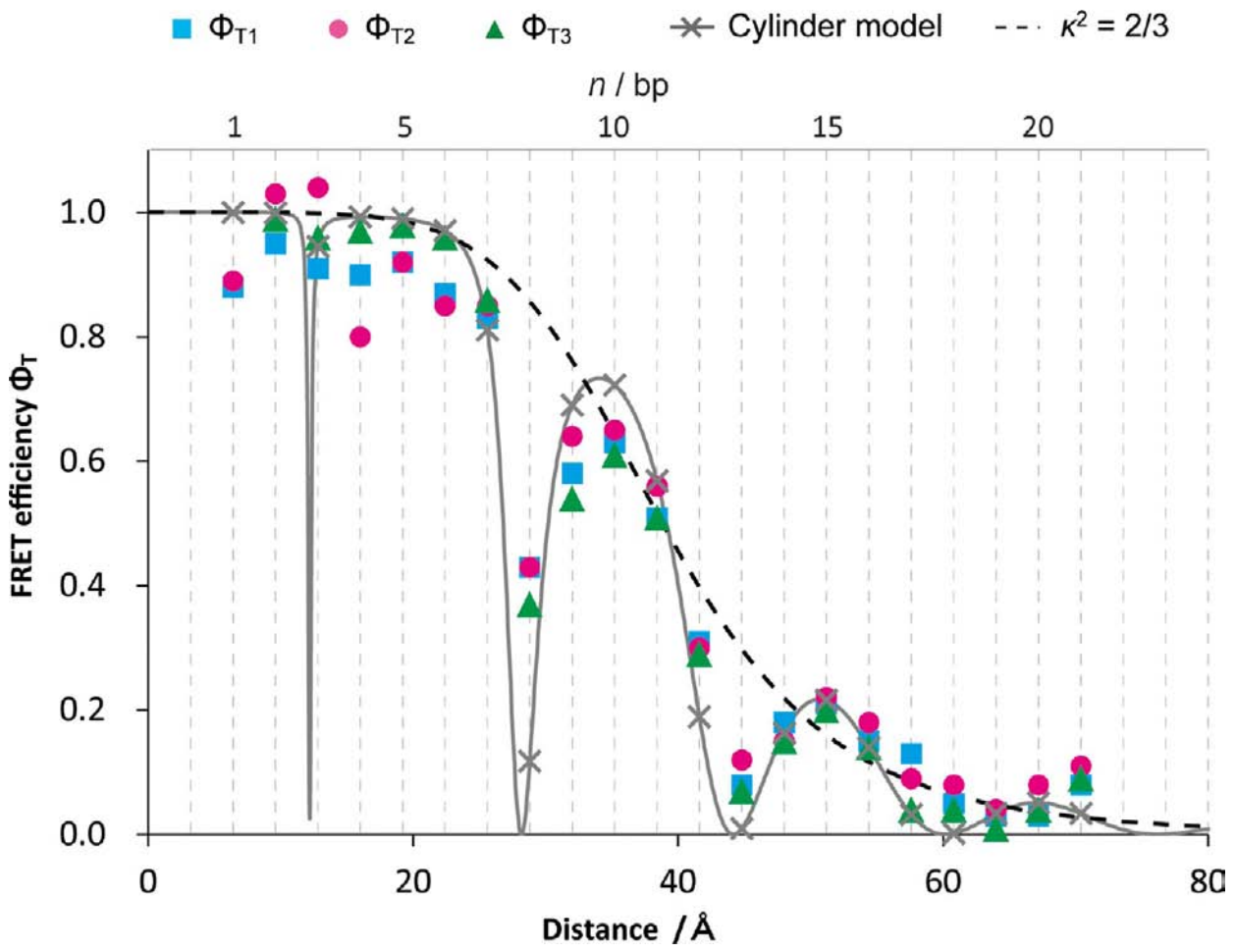

Figure 9. Comparison of FRET efficiency obtained from static fluorescence measurement (Φ_{T1}, cyan squares, Φ_{T2}, magenta circles) and time-resolved fluorescence spectroscopy (Φ_{T3}, green triangles) with theoretical values of cylinder model (gray line with cross symbols). The value of averaged orientation is also shown by dashed line.

coefficients calculated from the theoretical model and the experimental values were 0.957 for Φ_{T1}, 0.946 for Φ_{T2} and 0.962 for Φ_{T3}, indicating good agreement. Significant declines of Φ_T were observed at n = 8, 13, and 18; in these duplexes, the two chromophores (i.e., transition dipole moments) were in an approximately perpendicular orientation. The valley observed in Figure 9 was much deeper than valleys observed in other studies of duplexes with fluorophores attached at the termini. In our design, dyes are intercalated between base pairs. As a result, stacking interactions of dyes with neighboring base pairs suppress mobility of dyes. The deeper valley observed in our system is evidence of control of dye orientation. FRET efficiency in our system exhibit significant decline of ∼0.4 in FRET efficiency reflecting strong restriction of dye mobility. Such deep decline was also observed in FRET system using fluorescent nucleotide analog reported by Börjesson et al. In their system, fluorescent nucleotide analog was doubly fixed by stacking interaction and hydrogen bonding. Our system also showed similar deep decline of FRET efficiency, indicating that mobility of tethered dye within DNA duplex was strictly suppressed. Our DNA modified with base-surrogate chromophores provides a FRET model system that precisely reflects the orientation factor as well as distance, and FRET efficiency can be accurately predicted from a simplified cylinder model of the DNA helix.

From our results, we could further confirm the importance of the orientation factor. The effect of orientation factor should be carefully considered in FRET measurement because disregard of the orientation factor by using averaged value of $\kappa^2 = 2/3$ would cause a considerable error in distance estimation. Hence attention should be paid to unexpected restriction of dye mobility (e.g., groove binding) even though long flexible linkers are used to tether donor and acceptor dyes.

There was a relatively large difference between experimental and calculated Φ_T for duplexes with n = 1 and n = 8. In the case of the 1*a*/1*b* duplex, the experimental Φ_T was about 0.9, whereas the calculated value was 1.0. The acceptor emission was likely quenched due to the exciton coupling between the dyes due to the close proximity of P and E as they are separated by only one AT pair.[44] 1*a*/1*b* showed bathochromicity of perylene absorption in UV−vis spectra with respect to those of other duplexes (Figure S5). For the duplex with n = 8, Φ_T was calculated as ∼0.1 based on the cylinder model because transition dipole moments were nearly perpendicular. However, experimental Φ_Ts were about 0.4. When the θ_T is around 90°, the orientation factor (κ^2) becomes close to 0. Even small difference in θ_T would cause a large difference in κ^2.

In this study, we separated chromophores with AT base pairs to avoid sequence-dependent quenching of fluorescence. AT tracts are known to induce the curvature in a DNA duplex. However, because the curvature of AT tract is slight (5°/6 bp),[41]

dx.doi.org/10.1021/ja309279w | J. Am. Chem. Soc. 2013, 135, 741−750

the difference in orientation factor induced by the AT tract should be small.[17] In addition, the curvature will compensate as the AT tract is lengthened. Accordingly, we conclude that the effect of AT tract curvature was negligible in our system.

CONCLUSIONS

We have successfully developed a robust FRET system in which dye orientation and distance between chromophores are controlled within a rigid DNA duplex. FRET efficiency depended on the orientation of dyes as well as the distance, demonstrating that mobilities of the dyes were restricted by strong stacking interactions with neighboring base pairs. Experimental FRET efficiencies of our system were in good agreement with theoretical values predicted by the cylinder model of a DNA helix. The orientation factor, which is obscure due to difficulty of strict control of orientation, was reflected in our FRET system. In general, FRET is used to determine the distance between dyes. The results presented in this paper demonstrated that relative orientation of dyes strongly affects the FRET efficiencies. Our system using D-threoninol as a scaffold of functional molecule will be suitable for experimental verification of theoretical predictions. It can be also applied to structural analyses (such as helical pitch) of supramolecules and artificial helical polymers as well as oligonucleotides.

ASSOCIATED CONTENT

Supporting Information

List of symbols and their definition, UV−vis and CD spectra of P and E conjugated ODNs, fluorescence spectra and curve fitting data of all types (n = 1−21) of FRET duplex, fluorescence spectra quenched by GC basepair are available. These materials are available free of charge via the Internet at http://pubs.acs.org.

AUTHOR INFORMATION

Corresponding Author

kashida@nubio.nagoya-u.ac.jp; asanuma@nubio.nagoya-u.ac.jp

Notes

The authors declare no competing financial interest.

ACKNOWLEDGMENTS

This work was supported by a Grant-in-Aid for Scientific Research (A) (21241031), a Grant-in-Aid for Scientific Research on Innovative Areas "Nanomedicine Molecular Science" (no. 2306) from the Ministry of Education, Culture, Sports, Science, and Technology, Japan. Grant-in-Aid for Japan Society for the Promotion of Science Fellows [no. 227957] is also acknowledged.

REFERENCES

(1) (a) Förster, T. *Naturwissenschaften* **1946**, *6*, 166−175. (b) Jares-Erijman, E. A.; Jovin, T. M. *Nat. Biotechnol.* **2003**, *21*, 1387−1395. (c) Preus, S.; Wilhelmsson, L. M. *ChemBioChem* **2012**, *13*, 1990−2001.

(2) Sapsford, K. E.; Berti, L.; Medintz, I. L. *Angew. Chem. Int. Ed.* **2006**, *45*, 4562−4588.

(3) Selvin, P. R. *Methods Enzymol.* **1995**, *246*, 300−334.

(4) Stein, I. H.; Schüller, V.; Böhm, P.; Tinnefeld, P.; Liedl, T. *Chem. Phys. Chem.* **2011**, *12*, 689−695.

(5) Grunwell, J. R.; Glass, J. L.; Lacoste, T. D.; Deniz, A. A.; Chemla, D. S.; Schultz, P. G. *J. Am. Chem. Soc.* **2001**, *123*, 4295−4303.

(6) Kikuchi, K.; Takakusa, H.; Nagano, T. *TrAC, Trends Anal. Chem.* **2004**, *26*, 407−415.

(7) Mcdowell, S. E.; Jun, J. M.; Walter, N. G. *RNA* **2010**, *16*, 2414−2426.

(8) Shu, D.; Zhang, H.; Petrenko, R.; Meller, J.; Guo, P. *ACS Nano* **2010**, *4*, 6843−6853.

(9) Valeur, B. *Molecular Fluorescence*; Willy-VCH: Weinheim, 2002.

(10) Lakowicz, J. R. *Principles of Fluorescence Spectroscopy*, 3rd ed.; Springer: New York, 2006, p 445.

(11) Clegg, R. M. *Methods Enzymol.* **1992**, *211*, 353−388.

(12) Norman, D. G.; Grainger, R. J.; Uhrin, D.; Lilley, D. M. J. *Biochemistry* **2000**, *39*, 6317−6324.

(13) Masuko, M.; Ouchi, S.; Sode, K.; Ohtani, H.; Shimadzu, A. *Nucleic Acids Res.* **2000**, *28*, e34.

(14) Widengren, J.; Schweinberger, E.; Berger, S.; Seidel, C. A. M. *J. Phys. Chem. A* **2001**, *105*, 6851−6866.

(15) Dietrich, A.; Buschmann, V.; Müller, C.; Sauer, M. *Rev. Mol. Biotechnol.* **2002**, *82*, 211−231.

(16) Lee, S.; Lee, J.; Hohng, S. *PLoS One* **2010**, *5*, e12270.

(17) Di Fiori, N.; Meller, A. *Biophys. J.* **2010**, *98*, 2265−2272.

(18) Flehr, R.; Kienzler, A.; Bannwarth, W.; Kumke, M. U. *Bioconjugate Chem.* **2010**, *21*, 2347−2354.

(19) Kupstat, A.; Ritschel, T.; Kumke, M. U. *Bioconjugate Chem.* **2011**, *22*, 2546−2557.

(20) Lewis, F. D.; Zhang, L.; Zuo, X. *J. Am. Chem. Soc.* **2005**, *127*, 10002−10003.

(21) Iqbal, A.; Arslan, S.; Okumus, B.; Wilson, T. J.; Giraud, G.; Norman, D. G.; Ha, T.; Lilley, D. M. J. *Proc. Natl. Acad. Soc. U.S.A.* **2008**, *105*, 11176−11181.

(22) Li, X.; Yin, Y.; Yang, X.; Zhi, Z.; Zhao, X. S. *Chem. Phys. Lett.* **2011**, *513*, 271−275.

(23) Ouellet, J.; Schorr, S.; Iqbal, A.; Wilson, T. J.; Lilley, D. M. J. *Biophys. J.* **2011**, *101*, 1148−1154.

(24) Rindermann, J. J.; Akhtman, Y.; Richardson, J.; Brown, T.; Lagoudakis, P. G. *J. Am. Chem. Soc.* **2011**, *133*, 279−285.

(25) Urnavicius, L.; McPhee, S. A.; Lilley, D. M. J.; Norman, D. G. *Biophys. J.* **2012**, *102*, 561−568.

(26) Börjesson, K.; Preus, S.; El-Sapheer, A. H.; Brown, T.; Albinsson, B.; Wilhelmsson, L. M. *J. Am. Chem. Soc.* **2009**, *131*, 4288−4293.

(27) Kashida, H.; Liang, X. G.; Asanuma, H. *Curr. Org. Chem.* **2009**, *13*, 1065−1084.

(28) Kashida, H.; Takatsu, T.; Sekiguchi, K.; Asanuma, H. *Chem.—Eur. J.* **2010**, *16*, 2479−2486.

(29) Lindegaard, D.; Madsen, A. S.; Astakhova, I. V.; Malakhov, A. D.; Babu, B. R.; Korshun, V. A.; Wengel, J. *Bioorg. Med. Chem.* **2008**, *16*, 94.

(30) Liang, X. G.; Nishioka, H.; Mochizuki, T.; Asanuma, H. *J. Mater. Chem.* **2010**, *20*, 575−581.

(31) Kashida, H.; Asanuma, H. *Phys. Chem. Chem. Phys.* **2012**, *14*, 7196−7204.

(32) Liang, X. G.; Asanuma, H.; Kashida, H.; Takasu, A.; Sakamoto, T.; Kawai, G.; Komiyama, M. *J. Am. Chem. Soc.* **2003**, *125*, 16408−16415.

(33) Asanuma, H.; Hayashi, H.; Zhao, J.; Liang, X. G.; Yamazawa, A.; Kuramochi, T.; Matsunaga, D.; Aiba, Y.; Kashida, H.; Komiyama, M. *Chem. Commun.* **2006**, 5062−5064.

(34) Asanuma, H.; Akahane, A.; Kondo, N.; Osawa, T.; Kato, T.; Kashida, H. *Chem. Sci.* **2012**, *3*, 3165−3169.

(35) Sau, S. P.; Hrdlicka, P. J. *J. Org. Chem.* **2012**, *77*, 5−16.

(36) Fujii, T.; Kashida, H.; Asanuma, H. *Chem.—Eur. J.* **2009**, *15*, 10092−10102.

(37) (a) Kubista, M.; Åkerman, B.; Nordén, B. *J. Phys. Chem.* **1988**, *92*, 2352−2356. (b) Lyng, R.; Rodger, A.; Nordén, B. *Biopolymers* **1992**, *32*, 1201−1214. (c) Pradhan, P.; Jernström, B.; Seidel, A.; Nordén, B.; Gräslund, A. *Biochemistry* **1998**, *37*, 4664−4673. (d) Nakamura, M.; Fukunaga, Y.; Sasa, K.; Ohtoshi, Y.; Kanaori, K.; Hayashi, H.; Nakano, H.; Yamana, K. *Nucleic Acids Res.* **2005**, *33*, 5887−5895.

(38) Kypr, J.; Kejnovská, I.; Renčiuk, D.; Vorlíčková, M. *Nucleic Acids Res.* **2009**, *37*, 1713−1725.

(39) Teo, Y. N.; Kool, E. T. *Bioconjugate Chem.* **2009**, *20*, 2371−2380.
(40) Clegg, R. M.; Murchie, A. I. H.; Zechel, A.; Lilley, D. M. J. *Proc. Natl. Acad. Sci. U.S.A.* **1993**, *90*, 2994−2998.
(41) MacDonald, D.; Herbert, K.; Zhang, X.; Polgruto, T.; Lu, P. *J. Mol. Biol.* **2001**, *306*, 1081−1098.
(42) Wang, C.; Xu, J.; Weiss, R. G. *J. Phys. Chem. B* **2003**, *107*, 7015−7025.
(43) Tanizaki, Y.; Yoshinaga, T.; Hiratsuka, H. *Spectrochim. Acta, Part A* **1978**, *34*, 205−210.
(44) Asanuma, H.; Fujii, T.; Kato, T.; Kashida, H. *J. Photochem. Photobiol., C* **2012**, *13*, 124−135.